



# Carbon dots as solid-state electron mediator for BiVO<sub>4</sub>/CDs/CdS Z-scheme photocatalyst working under visible light

Xiuqin Wu<sup>1</sup>, Juan Zhao<sup>1</sup>, Liping Wang, Mumei Han, Mengling Zhang, Huibo Wang, Hui Huang\*, Yang Liu\*, Zhenhui Kang\*

Jiangsu Key Laboratory for Carbon-Based Functional Materials & Devices, Institute of Functional Nano & Soft Materials (FUNSOM), Soochow University, 199 Ren'ai Road, Suzhou, 215123, Jiangsu, PR China



## ARTICLE INFO

### Article history:

Received 26 November 2016

Received in revised form 14 January 2017

Accepted 18 January 2017

Available online 28 January 2017

### Keywords:

Carbon dots

Solid-state electron mediator

Z-scheme

Photocatalyst

Overall water splitting

## ABSTRACT

Z-scheme photocatalytic system is an efficient way to achieve high efficiency photocatalytic overall water splitting. However, the acquisition of efficient Z-scheme visible-light photocatalysts is still a huge challenge at present due to the inactive visible light-active component and various low-band-gap for semiconductors. Herein, we constructed the BiVO<sub>4</sub>/CdS/CdS Z-scheme photocatalyst with carbon dots (CDs) as solid-state electron mediator, which exhibits excellent photocatalytic activity and stability for photocatalytic overall water splitting under visible light. The BCC50 (BiVO<sub>4</sub>/CdS/CdS with the mass ratio of BiVO<sub>4</sub>/CdS = 50%) as photocatalyst shows the best photocatalytic activity with stoichiometric ratio of H<sub>2</sub> evolution rate of 1.24 μmol/h and O<sub>2</sub> evolution rate of about 0.61 μmol/h. The enhanced photocatalytic activity of the Z-scheme photocatalyst can be attributed to high efficiencies for separation and transport of photogenerated charge carriers and extended the lifetime of electrons and holes.

© 2017 Elsevier B.V. All rights reserved.

## 1. Introduction

Photocatalytic water splitting into H<sub>2</sub> and O<sub>2</sub> based on semiconductor photocatalysts is considered as a promising approach for converting solar energy into chemical energy [1–4]. There are two dominant ways to achieve overall water splitting: the first one is the use of single photocatalysts, which require the photocatalysts possess smaller overpotential and higher photocatalytic activity. While the other one is the development of Z-scheme photocatalytic systems. Compared with single photocatalysts, Z-scheme photocatalytic system is simpler and more effective. A Z-scheme system is constructed of two photocatalysts with/without an electron mediator, in which one can generate H<sub>2</sub> and the other can produce O<sub>2</sub> [5–9]. For an efficient Z-scheme visible-light photocatalyst, a solid electron mediator is more favourable on the basis of recovery of the photocatalyst. However, it's difficult that a solid-state electron mediator lied in achieving a dynamic equilibrium between the electron-accepting and -donating abilities of the mediator, allowing to remain relatively unchanged during reaction [5,8]. Hence, the efficient Z-scheme visible-light photocatalysts are still limited,

and the inactive visible light-active component and various low-band-gap for semiconductors are mainly restricted the practical application [2,10]. At present, it's urgent to exploring novel visible-light active components to construct and develop a highly efficient Z-scheme photocatalytic system for overall water splitting.

Monoclinic bismuth vanadate (m-BiVO<sub>4</sub>) with a narrow band gap of about 2.4 eV has been reported to own excellent activity of water splitting under visible light for O<sub>2</sub> evolution due to the favourable valence band position (formed by Bi 6s or a hybrid orbital of Bi 6s and O 2p) [11]. Cadmium sulfide (CdS), a fascinating visible light material with a band gap of around 2.4 eV, can be used for H<sub>2</sub> production from water splitting owing to the suitable favourable conduction band position. However, the photocatalytic efficiency for H<sub>2</sub> production of CdS is severely limited because of the fast charge recombination and photocorrosion of CdS [12,13].

Carbon dots (CDs), as an appealing group of zero-dimensional nanostructures, possess chemical stability, low cost, unique photo-induced electron transfer and electron reservoir properties. They show satisfactory performances as a catalyst component or a catalyst in overall water splitting, hydrogen generation, photoelectric conversion and so on [14–19]. The CD–carbon nitride nanocomposite demonstrates great photocatalytic performance for complete water splitting into H<sub>2</sub> and O<sub>2</sub> [19]. The CDs could as an electron transfer intermediary to significantly improve the photoelectric conversion efficiency [15]. Therefore, the CDs maybe an ideal elec-

\* Corresponding authors.

E-mail addresses: [hhuang0618@suda.edu.cn](mailto:hhuang0618@suda.edu.cn) (H. Huang), [\(Y. Liu\), \[\\(Z. Kang\\).\]\(mailto:zhkang@suda.edu.cn\)](mailto:yangl@suda.edu.cn)

<sup>1</sup> These authors contributed equally to this work.

tron mediator to construe Z-scheme system. Based on the above, coupling of BiVO<sub>4</sub>, CdS and CDs generates a solid-state Z-scheme system may efficiently reduce the recombination of photoexcited charge carriers and enhance the photocatalytic activity for water splitting [20–22].

Herein, we designed a promising solid-state BiVO<sub>4</sub>/CDs/CdS Z-scheme, in which BiVO<sub>4</sub> and CdS nanoparticles can serve as O<sub>2</sub> evolution and H<sub>2</sub> evolution photocatalysts, respectively, and CDs can be used as solid electron mediator for photocatalytic water splitting under visible-light illumination. We demonstrate the as-prepared BiVO<sub>4</sub>/CDs/CdS photocatalyst shows enhanced photocatalytic activity and improved stability for splitting water into H<sub>2</sub> and O<sub>2</sub> with stoichiometric ratio (H<sub>2</sub> evolution rate of 1.24 μmol/h and O<sub>2</sub> evolution rate of about 0.61 μmol/h). The enhanced photocatalytic activity of the Z-scheme photocatalyst can be attributed to high efficiencies for separation and transport of photogenerated charge carriers and extended the lifetime of electrons and holes.

## 2. Experimental section

All the chemicals were analytical grade and used without further purification.

### 2.1. Synthesis of BiVO<sub>4</sub>/CDs

CDs were prepared via an electrochemical etching method reported in the previous work [23]. BiVO<sub>4</sub>/CDs were synthesized through hydrothermal method [24]. Typically, 5 mM Bi(NO<sub>3</sub>)<sub>3</sub>·5H<sub>2</sub>O was completely dissolved in 20 mL of 2 M HNO<sub>3</sub>. Then, under stirring, 10 mL of 2 M NaOH containing NH<sub>4</sub>VO<sub>3</sub> (5 mM) was dropwise added into the above solution to form a yellow suspension. The pH value of the obtained yellow suspension was adjusted to 7 using 1 M NaOH solution and continue stirring for 30 min. After that, about 48.6 mg CDs were added into the above yellow suspension (pH = 7), followed by ultrasound for 30 min. The resultant mixture was then transferred to Teflon-lined autoclaves and maintained at 180 °C for 12 h. The autoclaves were then allowed to cool down to room temperature. Finally, the resultant solid was separated by centrifugation and washed with water several times and then dried in the air. The pure BiVO<sub>4</sub> sample was synthesized under the same conditions without CDs.

### 2.2. Synthesis of BiVO<sub>4</sub>/CDs/CdS

The BiVO<sub>4</sub>/CDs/CdS was prepared by a facile precipitation method [5]. 0.3 g of BiVO<sub>4</sub>/CDs and a certain CdCl<sub>2</sub> were successively added to 30 mL of distilled water, and then a certain volume of 50 mM Na<sub>2</sub>S aqueous solution was dropwise added into the above solution. After stirring 2 h, the precipitate was finally collected by centrifugation, washed several times with deionized water and then dried at 80 °C for 24 h. The weight ratios of BiVO<sub>4</sub> to CdS were R = 0, 10, 30, 50, 80, and 100, which are labelled as BCC0, BCC10, BCC30, BCC50, BCC80, and BCC100, respectively. The pure CdS sample was synthesized under the same conditions without BiVO<sub>4</sub>/CDs.

### 2.3. Characterization

X-ray diffractograms (XRD) were recorded with a PIXcel3D X-ray diffractometer (Empyrean, Holland Panalytical) using Cu Kα radiation ( $\lambda = 0.154178$  nm). Transmission electron microscopic (TEM) measurements were performed by a FEI-Tecnai F20 transmission electron microscope with an accelerating voltage of 200 kV. UV-vis diffuse reflection spectra (DRS) of the samples were taken using a Cary 60 spectrophotometer in the wavelength range of 200–800 nm. The photoluminescence (PL) spectra were measured

with a Horiba Jobin Yvon (Fluoro Max-4) luminescence spectrometer (excitation wavelength = 340 nm) at room temperature in air. The transient time-resolved photoluminescence (PL) decay measurements were carried out by a Fluorolog-TCSPC luminescence spectrometer with an excitation wavelength of 340 nm. The Fourier transform infrared (FTIR) spectra of the samples were obtained with a Nicolet 6700 spectrophotometer in the scan range of 400–4000 cm<sup>-1</sup>. The surface properties of the samples were determined by KRATOS Axis ultra-DLD X-ray photoelectron spectroscope (XPS) with a monochromatized Mg Kα X-ray source ( $h\nu = 1283.3$  eV). Ultraviolet photoelectron spectroscopy (UPS) measurements of the as-prepared samples were performed with He I (21.22 eV) as monochromatic light source and a total instrumental energy resolution of 100 meV. Raman spectra were recorded with a HR 800 Raman spectrometer (J Y, France) under an excitation of 514 nm laser light.

The photoelectrochemical characteristics were performed on a CHI 920C workstation (CH Instruments, Chenzhou, Shanghai, China) using a standard three-compartment cell with a platinum wire as reference electrode and a saturated calomel electrode (SCE) as counter electrode. The photocurrent measurements were measured at open circuit potential in ultrapure water and a 300 W Xe lamp positioned 2 cm away from the working electrode was used as the light source. The electrochemical impedance spectroscopy (EIS) measurements were carried out at open circuit potential with an AC amplitude of 10 mV from 100 Hz to 1 MHz in ultrapure water.

### 2.4. Photocatalytic reaction

The Pyrex glass photoreactor was applied to test the photocatalytic H<sub>2</sub> production, which connected with a closed gas-circulation system. The 80 mg sample as photocatalyst was added into 100 mL ultrapure water, then the mixed liquor was transferred to the above photoreactor. The temperature of photocatalytic reaction was held at 25 °C by cyclic water installation. The light source was provided by 300 W Xe-lamp (PLS-SXE 300, Beijing Trusttech Co. Ltd, China) coupled with a cutoff filter (Kenko L-42,  $\lambda > 420$  nm) and the area of irradiation was 4.27 cm<sup>2</sup>. The amount of H<sub>2</sub> was obtained on gas chromatography (GC-7900, Ar as a carrier gas) set up with a 5 Å molecular sieve column and a thermalconductivity detector (TCD). The temperatures of GCoven, injection and detector were 80, 100, and 120 °C, respectively. Meanwhile, the photocatalytic overall water splitting was also detected by sealed bottle with 20 mg (different samples as photocatalysts) and 20 mL ultrapure water. The light source was offered with PCX50A Discover multichannel photocatalytic reaction device by PerfectLight technology co., LTD. Then the gases generated was also detected by gas chromatography (GC-7890T, 5 Å molecular sieve column, TCD detector).

## 3. Results and discussion

The phase and crystal structure of the as-prepared samples were investigated by XRD. Fig. 1 shows XRD patterns of the BiVO<sub>4</sub>, CdS and BCC50. As can be seen, the as-obtained BiVO<sub>4</sub> is highly crystalline and can be indexed to the structure of monoclinic BiVO<sub>4</sub> (JCPDS No. 14-0688) [11,25,26]. The XRD pattern of CdS matches well with cubic phase of CdS (JCPDS No. 89-0440) [27]. Two characteristic peaks at approximately 26° and 43° found in the XRD pattern of CDs (Fig. 3b) can be assigned to the (002) and (101) planes of graphitic carbon, respectively [23]. For the XRD pattern of BCC50, the diffraction peaks for CdS and diffraction peaks corresponding to the monoclinic BiVO<sub>4</sub> are observed and the position of peaks is unchanged. In addition, no diffraction peak of CDs at approximately 26° or 43° is observed in the Z-scheme BCC50, which could be ascribed to the small amount and relatively low

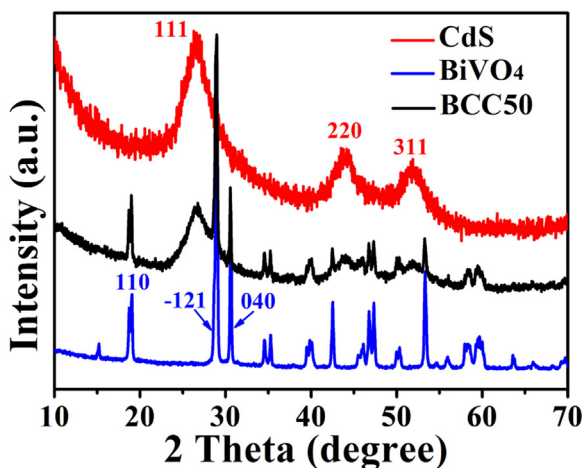


Fig. 1. XRD patterns of BiVO<sub>4</sub>, CdS and BCC50.

diffraction intensity of CDs [14,19,28,29]. These results confirmed that the BiVO<sub>4</sub>/CDs/CdS composites were successfully synthesized. Moreover, no other diffraction peaks were found in the samples, indicating the high purity of the as-prepared samples.

The FTIR spectra of CDs, BiVO<sub>4</sub>, CdS and BCC50 are shown in Fig. 2a. The bond located at around 3445 cm<sup>-1</sup> in all four spectra can be attributed to stretching vibrations of the adsorbed H<sub>2</sub>O [30]. The FTIR spectrum of CDs exhibits several strong characteristic peaks at 1045, 1400 and 1636 cm<sup>-1</sup>, which may be ascribed to the typical stretching vibration of C—O—C, —COO and C=C/C=O, respectively [19,31]. In the FTIR spectrum of BiVO<sub>4</sub>, the peak at 1390 cm<sup>-1</sup> is corresponding to trace NO<sub>3</sub><sup>-</sup> (remaining reactant) [32,33]. The strong absorption peak at 725 cm<sup>-1</sup> can be assigned to  $\nu_1(\text{VO}_4)$

and  $\nu_3(\text{VO}_4)$  [34]. Meanwhile, the peak at 1630 cm<sup>-1</sup> may assign to the stretching vibrations of the adsorbed H<sub>2</sub>O [32,35]. For CdS, the absorption peak at 1622 cm<sup>-1</sup> should be attributed to the surface-adsorbed H<sub>2</sub>O [35]. The typical characteristic absorption bands at 1387 and 1115 cm<sup>-1</sup> are due to the vibrations of Cd-S bond [36]. The FTIR spectrum of BCC50 composite represents the overlap spectra of all CDs, BiVO<sub>4</sub> and CdS. These results further demonstrated that the BiVO<sub>4</sub>/CDs/CdS composites were successfully synthesized. The Raman spectra of CDs, BiVO<sub>4</sub>, CdS and BCC50 are shown in Fig. 2b. The Raman spectrum of CDs reveals that two characteristic peaks at about 1350 and 1600 cm<sup>-1</sup> are correspond to D-band (the sp<sup>3</sup> defects of carbon atoms) and G-band (the sp<sup>2</sup> bonded carbon atoms), respectively [37]. The Raman spectrum of BiVO<sub>4</sub> displays five Raman peaks at around 211, 326, 367, 716, and 827 cm<sup>-1</sup>, which proves that BiVO<sub>4</sub> is monoclinic phase [37]. The Raman spectrum of CdS exhibits two characteristic peaks at about 300 and 600 cm<sup>-1</sup>, assigning to the first order longitudinal optic phonon (1LO) and the second-order phonon (2LO), respectively [38,39]. The Raman spectrum of the BCC50 composite shows a combination of characteristic bands of CDs, BiVO<sub>4</sub> and CdS, which demonstrated that BiVO<sub>4</sub>/CDs/CdS Z-scheme structure was successfully constructed.

The microstructure and morphology of the as-obtained samples were investigated by TEM and HRTEM. The TEM images of the as-prepared CDs, BiVO<sub>4</sub>, CdS and BCC50 samples are shown in Figs. 3 and 4. Fig. 3a shows the TEM image of synthesized CDs, which indicated that CDs are uniform with about 5 nm in diameter. The HRTEM image of CDs (insert in Fig. 3a) exhibits lattice spacing is 0.21 nm, assigning to in-plane (100) lattice plane of graphitic carbon [35,40]. In Fig. 4a, it can be seen that the surface of BiVO<sub>4</sub> is smooth, and it displays a sphere-like morphology with average diameter about 100–150 nm. The HRTEM image of BiVO<sub>4</sub> (Fig. 4b) shows the lattice space of 0.24 nm is corresponding to the (020)

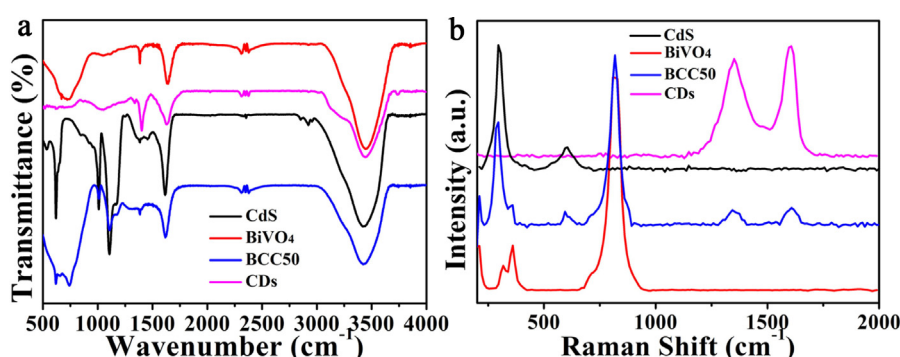


Fig. 2. (a) FTIR spectra and (b) Raman spectra of CDs, BiVO<sub>4</sub>, CdS and BCC50.

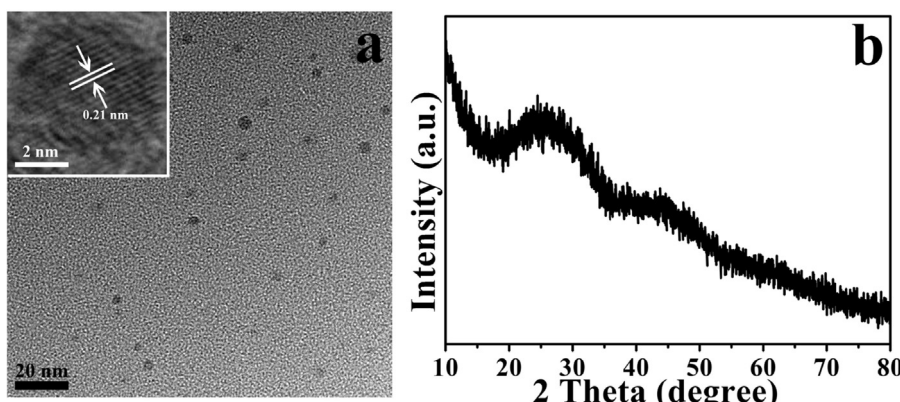
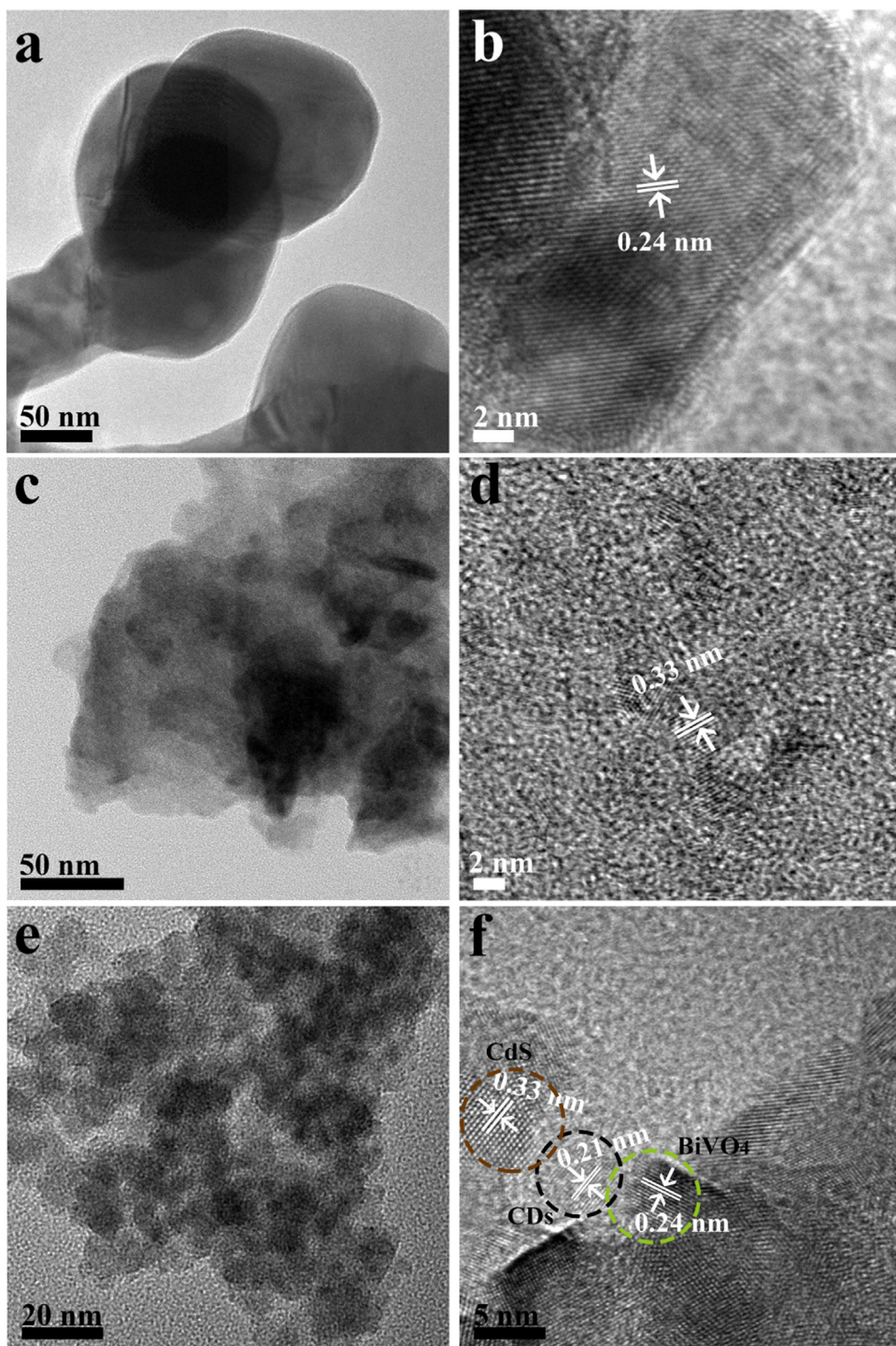


Fig. 3. (a) TEM image of CDs, the insert is HRTEM image of CDs. (b) XRD spectrum of CDs.



**Fig. 4.** (a) TEM image and (b) HRTEM image of  $\text{BiVO}_4$ . (c) TEM image and (d) HRTEM image of CdS. (e) TEM image and (d) HRTEM image of BCC50.

crystallographic planes of the monoclinic  $\text{BiVO}_4$  [41]. The TEM image of CdS in Fig. 4c indicates the obtained CdS is flake-like shape. As shown in the HRTEM image of CdS (Fig. 4d), the lattice space of CdS can be identified as 0.33 nm, corresponding to the (111) spacing of cubic CdS [8]. The TEM image of BCC50 is shown in Fig. 4e, suggesting that the as-prepared BCC50 is irregular morphology. The representative HRTEM image of BCC50 is presented in Fig. 4f. The measured lattice spaces of 0.24, 0.21, 0.33 nm match well with the (020) plane of monoclinic  $\text{BiVO}_4$ , the (100) plane of graphitic carbon and the (111) plane of cubic CdS, respectively [14,41,42]. The inti-

mate contact of  $\text{BiVO}_4$ , CdS and CDs is beneficial to charge transport and photocatalytic activity.

The chemical compositions and valence states of the BCC50 were investigated by XPS. The survey XPS spectrum of the as-prepared BCC50 sample is shown in Fig. 5a, which indicated that the main elements on the surface of the BCC50 are C, Bi, V, Cd, S. Fig. 5b displays the C 1s spectrum of the BCC50, which can be divided into three peaks located at 284.6, 286.3, and 288.4 eV, corresponding to C–C, C–O–C, and C=O, respectively [43–45]. The XPS signals of O 1s are observed at binding energies of 529.8, 530.4 and 532.2 eV (Fig. 5c), which ascribed to the lattice oxygen of layer-structured

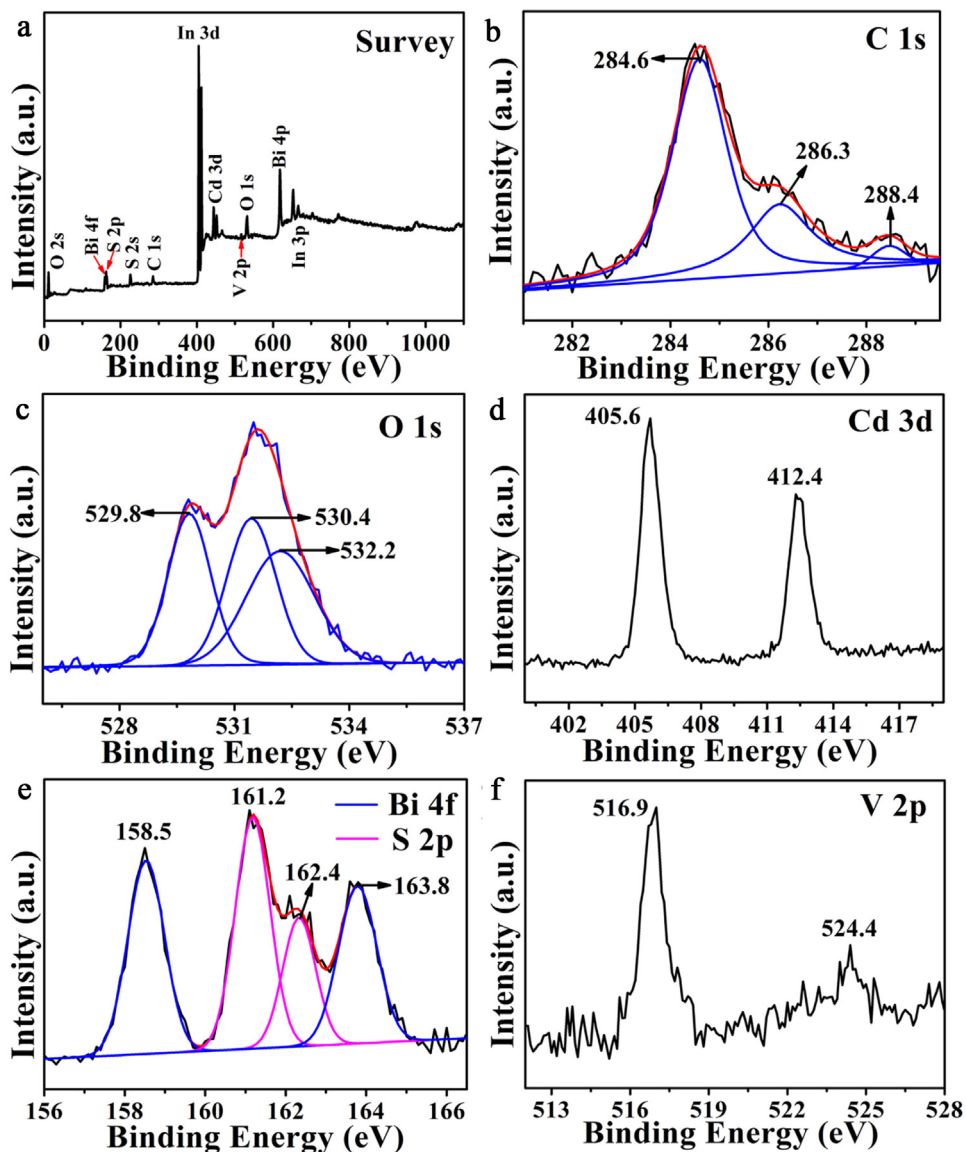


**Fig. 5.** Survey XPS spectrum (a) and High-resolution XPS spectra of C 1s (b), O 1s (c), Cd 3d (d), Bi 4f/S 2p (e) and V 2p (f).

$\text{Bi}_2\text{O}_2^{2+}$ , surface adsorbed  $\text{H}_2\text{O}$  and  $\text{C}-\text{O}/\text{C}=\text{O}$ , respectively [37,46]. The high resolution spectra of Cd 3d (Fig. 5d) present two peaks at 405.6 (Cd 3d3/2) and 412.4 eV (Cd 3d5/2), which indicate that the Cd species exist as +2 [47,48]. In Fig. 5e, two peaks (blue trace) at about 158.5 and 163.8 eV can be ascribed to Bi 4f 7/2 and Bi 4f 5/2, respectively, demonstrating that the valence state of Bi in the BCC50 is +3 [49]. And the other two peaks (pink trace) at around 161.2 and 162.5 eV were attributed to S 2p1/2 and S 2p3/2, respectively [8,50]. In Fig. 5f, the V 2p spectrum shows binding energies at 516.9 eV for V2p3/2 and 524.4 for V 2p1/2 [51,52]. According to the above XPS results, the Z-scheme  $\text{BiVO}_4/\text{CDs/CdS}$  photocatalytic system was successfully fabricated, which is consistent with XRD, TEM measurements.

The UV-vis diffuse reflectance spectra were used to determine the optical properties of samples. The UV-vis DRS of  $\text{BiVO}_4$ , CdS and BCC50 are presented in Fig. 6a. All these samples display almost the same absorption profile. The absorption edges of  $\text{BiVO}_4$  and CdS are approximately about 510 and 580 nm, respectively. In comparison with  $\text{BiVO}_4$  and CdS, the absorption edge of BCC50 exhibits an obvious redshift, probably owing to the interfacial interaction between CdS and CDs according to previous report. The results indicate that

BCC50 composite can enhance visible light absorption, which could result in the improvement of photocatalytic activity. The optical band gap of a semiconductor can be estimated from the following formula [19]:

$$(\alpha h\nu) = A(h\nu - E_g)^n/2$$

Where  $\alpha$ ,  $h$ ,  $\nu$ ,  $A$  and  $E_g$  are absorption coefficient, Planck's constant, light frequency, constant value and band gap energy, respectively. And  $n=1$  and 4 for direct and indirect transition type of materials, respectively. Due to  $\text{BiVO}_4$  and CdS are direct transition type of semiconductors, the direct band gaps of  $\text{BiVO}_4$  and CdS can be calculated from the plots of  $(\alpha h\nu)$  [2] versus  $(h\nu)$  (Fig. 6b). Therefore, the band gaps of pure  $\text{BiVO}_4$  and CdS are determined to be 2.44 and 2.38 eV, respectively.

Fig. 6c shows the UPS spectra of  $\text{BiVO}_4$  and CdS. The valence band energies ( $E_{VB}$ ) were determined to be 7.23 and 6.73 eV for  $\text{BiVO}_4$  and CdS, respectively, by subtracting the width of the He I UPS spectra from the excitation energy (21.22 eV) [19]. Furthermore, due to the  $E_g = E_{VB} - E_{CB}$ , the conduction band energies ( $E_{CB}$ ) of  $\text{BiVO}_4$  and CdS were thus determined to be 4.79 and 4.35 eV, respectively. Fig. 6d displays the band structure diagram for  $\text{BiVO}_4$

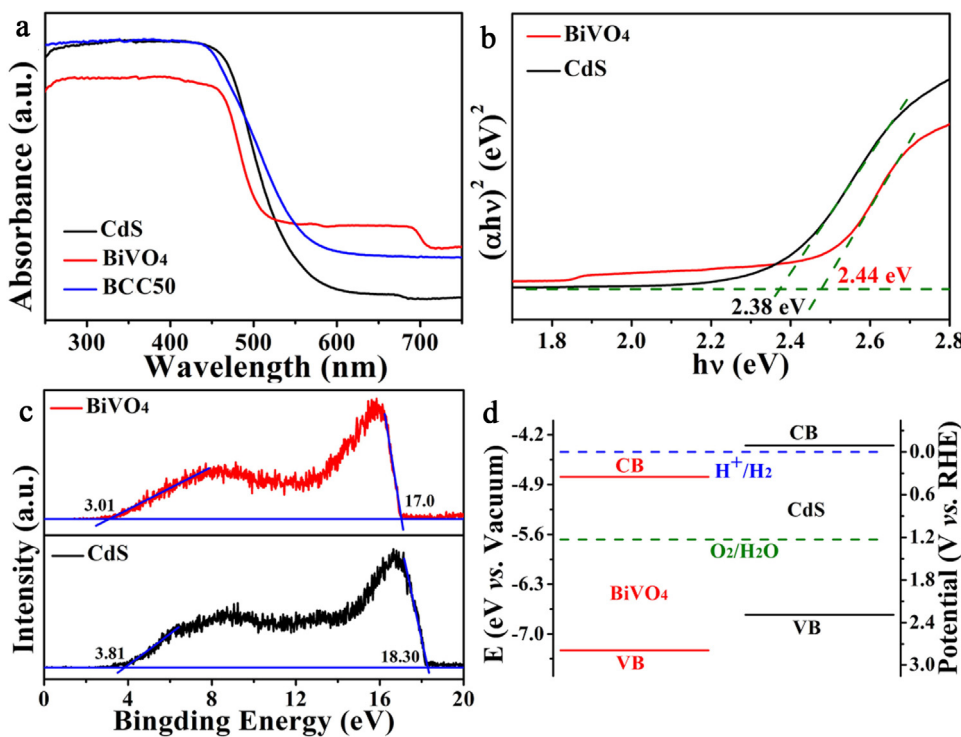


**Fig. 6.** (a) UV–vis DRS spectra of BiVO<sub>4</sub>, CdS and BCC50. (b) Plots of  $(\alpha h\nu)^2$  versus  $(h\nu)$  for BiVO<sub>4</sub> and CdS. (c) UPS spectra of BiVO<sub>4</sub> and CdS. (d) The band structure diagram of BiVO<sub>4</sub> and CdS.

and CdS. The  $E_{CB}$  and  $E_{VB}$  values in electron volts can be converted into electrochemical energy potentials in volts according to the reference standard that 0 V vs. RHE (reversible hydrogen electrode) equals  $-4.44$  eV vs. vacuum level. Therefore, the  $E_{VB}$  and  $E_{CB}$  of BiVO<sub>4</sub> were  $2.79$  and  $0.35$  V (vs. RHE), respectively, and the  $E_{VB}$  and  $E_{CB}$  of CdS were  $1.88$  and  $-0.09$  V (vs. RHE), respectively. Obviously, both the Ec and Ev levels of BiVO<sub>4</sub> are more positive than the reduction level for H<sup>+</sup>/H<sub>2</sub> (0 V vs. RHE) and the oxidation level for H<sub>2</sub>O/O<sub>2</sub> ( $1.23$  eV vs. RHE), respectively, thus the holes in the VB of BiVO<sub>4</sub> can theoretically oxidize H<sub>2</sub>O into O<sub>2</sub>. And the  $E_{CB}$  levels of CdS is more negative than the reduction level for H<sup>+</sup>/H<sub>2</sub> (0 V vs. RHE). Therefore, the electrons in the CB of CdS can participate in the H<sup>+</sup> reduction half reaction to generate H<sub>2</sub>. The results demonstrated that the Z-scheme BiVO<sub>4</sub>/CdS/CdS photocatalyst can realize complete water splitting into H<sub>2</sub> and O<sub>2</sub> [19].

The photocatalytic performances for water splitting into H<sub>2</sub> and O<sub>2</sub> of the as-prepared samples are shown in Fig. 7. No H<sub>2</sub> was observed with the BiVO<sub>4</sub> or BiVO<sub>4</sub>/CdS as a photocatalyst in pure water under visible light, which can be ascribed to lower conduction potential of BiVO<sub>4</sub>. Without light irradiation or photocatalyst, no H<sub>2</sub> was observed in water, which demonstrates that light and catalyst are essential prerequisites for photocatalytic water splitting. Fig. 7a shows the photocatalytic performances for gases evolution of BCC50. It can be seen that the BCC50 exhibited H<sub>2</sub> evolution rate of about  $1.24$  μmol/h and O<sub>2</sub> evolution rate of

about  $0.61$  μmol/h. The H<sub>2</sub> and O<sub>2</sub> evolution in a stoichiometric ratio indicates that this Z-scheme system can split water completely. The stable photocatalytic performance of BCC50 sample was confirmed, as shown in Fig. 8. In the tenth cycle experiments, the H<sub>2</sub> evolution rate could be well maintained ( $1.22$  μmol/h). The results revealed that the Z-scheme photocatalyst is stable and remains high photocatalytic performance in water splitting under visible light irradiation. Fig. 7b depicts the H<sub>2</sub> and O<sub>2</sub> evolution rates of as-prepared various samples. It can be found that the rates of H<sub>2</sub>/O<sub>2</sub> evolution of BCC0, BCC10, BCC30, BCC50, BCC80 and BCC100 were  $0.18/0.09$ ,  $0.46/0.22$ ,  $0.80/0.41$ ,  $1.24/0.61$ ,  $1.04/0.52$  and  $0.91/0.44$  μmol/h, respectively. Thereby, the BCC50 shows the best photocatalytic activity for water splitting among the prepared composites. Table 1 shows the photocatalytic water splitting performances of BiVO<sub>4</sub> or CdS Z-scheme systems, which suggests that BiVO<sub>4</sub>/CdS/CdS Z-scheme photocatalyst possess excellent photocatalytic activity over water splitting under visible light without co-catalyst or sacrificial agent [9,53].

The EIS measurements and PL spectra were further used to investigate the efficiency of separation and transfer of charge carriers. Fig. 7c describes the EIS (Nyquist plots) of BiVO<sub>4</sub>, CdS and BCC50 obtained in pure water. The high-frequency semicircle in the EIS corresponds to the electron transfer process at the interface between semiconductor and electrolyte, and a smaller semicircle radius revealed a higher charge transfer efficiency [54,55]. As can

**Table 1**

A survey of the photocatalytic water splitting performances of BiVO<sub>4</sub> or CdS Z-scheme systems.

Photocatalyst	co-catalyst	Light source (wavelength)	Solution	Rate of H <sub>2</sub> evolution (μmol/h)	Reference
BiVO <sub>4</sub> /CdS/CdS	No	λ > 420 nm	ultrapure water (100 mL)	1.24	This work
quantum sized BiVO <sub>4</sub>	No	solar light irradiation	pure water (200 mL)	0.22	[9]
BiVO <sub>4</sub> nanowires	2 wt.% Pt	λ > 420 nm	lactic acid (20 vol.%) solution or 1 M Na <sub>2</sub> SO <sub>3</sub> (200 mL)	0	[53]
CdS/BiVO <sub>4</sub> NWS	2 wt.% Pt	λ > 420 nm	lactic acid (20 vol.%) solution or 1 M Na <sub>2</sub> SO <sub>3</sub> (200 mL)	1153	[53]
CdS/BiVO <sub>4</sub> NWS	No	λ > 420 nm	lactic acid (20 vol.%) solution or 1 M Na <sub>2</sub> SO <sub>3</sub> (200 mL)	124	[53]
CdS nanoparticles	2 wt.% Pt	λ > 420 nm	lactic acid (20 vol.%) solution or 1 M Na <sub>2</sub> SO <sub>3</sub> (200 mL)	568	[53]

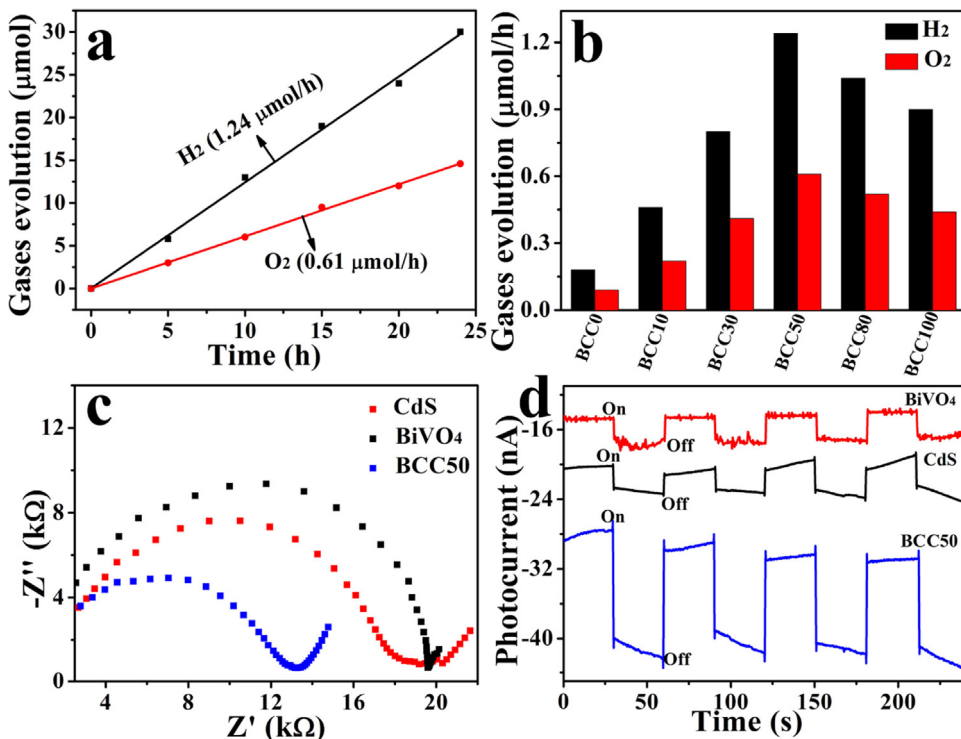


**Fig. 7.** (a) The photocatalytic activity of BCC50 under visible light irradiation for water splitting into  $H_2$  and  $O_2$ . (b)  $H_2$  and  $O_2$  evolution rates using various as-prepared samples as photocatalysts under visible light irradiation. (c) The EIS of  $BiVO_4$ ,  $CdS$  and BCC50. (d) The i-t curves of  $BiVO_4$ ,  $CdS$  and BCC50.

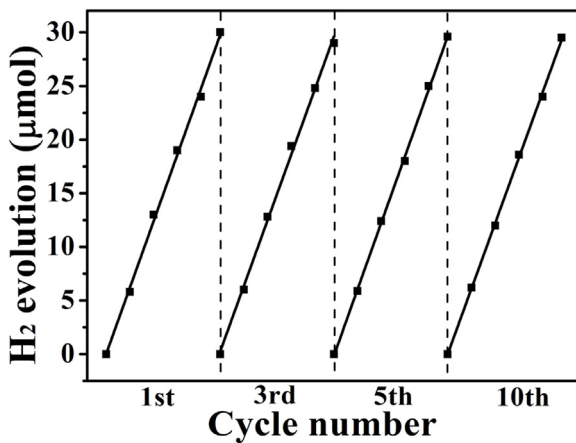


**Fig. 8.** The stability of photocatalytic water splitting used BCC50 as a photocatalyst.

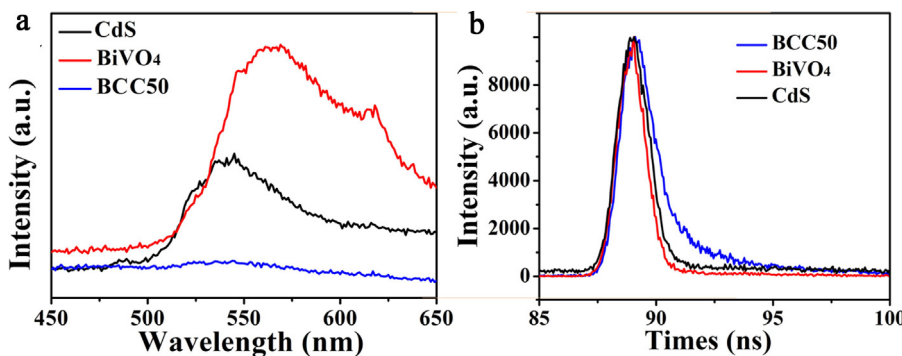
be seen from Fig. 7c, the semicircle radius for BCC50 is smaller than that for pure  $BiVO_4$  and  $CdS$ , implying that BCC50 possesses a higher efficiency for separation and transport of photogenerated charge carriers. The transient photocurrent techniques were further used to evaluate photoresponse performance of the samples. Fig. 7d shows the curves of transient photocurrent vs. time (i-t) of  $BiVO_4$ ,  $CdS$  and BCC50 with the period of light on/off every 30 s. Under the light illumination, all photoelectrodes show a sharp increase and reach to a steady state, while the photocurrent exhibits a dramatic decrease when the light turned off. The photocurrents of  $BiVO_4$ ,  $CdS$  and BCC50 were 2.7, 3.3 and 14.6 nA, respectively, during the light-on cycle. It can be obviously seen that BCC50 displays a remarkable improvement of photoresponse performance compared to that of  $BiVO_4$  and  $CdS$ , demonstrating that the Z-scheme  $BiVO_4/CDs/CdS$  is effective to prohibit the photogenerated charge recombination.

Fig. 9a shows the PL spectra of  $BiVO_4$ ,  $CdS$  and BCC50. It can be seen that  $BiVO_4$  exhibits a strong PL emission peak around 565 nm

and  $CdS$  presents a PL emission peak around 542 nm, which can be attributed to the recombination of electron-hole pairs. For BCC50, the PL intensity is obviously weaker than that of  $BiVO_4$  and  $CdS$ , indicating that the BCC50 can effectively hamper the recombination of photogenerated electron-hole pairs and further improve the photocatalytic activity [56].

To further understand the charge carrier transfer properties of our samples, the time-resolved PL spectrum was measured. Fig. 9b is the PL delay fitting curves of the BCC50,  $BiVO_4$  and  $CdS$ . The lifetime of  $BiVO_4$ ,  $CdS$  and BCC50 were 0.62, 0.76, 1.34 ns, respectively. A lifetime on the ns level implies the singlet state nature of emission of the samples [57]. This result proves our Z-scheme  $BiVO_4/CDs/CdS$  composite has improved separation efficiency of photogenerated electron-hole pairs and increased the lifetime of electrons and holes.

According to a lot of previous reports, CDs could be quenched efficiently by electron acceptor or donor molecules in solution, such as 2,4-dinitrotoluene (electron acceptor) and DEA (electron donor), which proved that CDs are good electron donors and electron acceptors [58,59]. This unique properties makes CDs a good electron mediator for Z-scheme system. To explain the enhanced photocatalytic activity of Z-scheme  $BiVO_4/CDs/CdS$ , a probable schematic mechanism is proposed, as shown in Fig. 10. Under the visible light illumination, both  $BiVO_4$  and  $CdS$  can absorb the visible light according to the UV spectra (Fig. 6a) and can be excited to generate electrons in the CB and holes in the VB. The photogenerated electrons in the CB of  $BiVO_4$  are able to migrate quickly to the surface of CDs and further transfer to the VB of  $CdS$  because of the photoinduced electron transfer property of CDs. Simultaneously, the holes in the VB of  $BiVO_4$  oxidize water to  $O_2$ . On the other hand, the photogenerated electrons in the CB of  $CdS$  can be used for reduce water to  $H_2$  due to  $E_{CB}$  of  $CdS$  ( $-0.09 \text{ V vs. RHE}$ ) are more negative than the standard redox potential of  $H^+/H_2$  ( $0 \text{ V vs. RHE}$ ). Therefore, the favourable transfer of photogenerated electrons and holes in  $BiVO_4/CDs/CdS$  can effectively suppress recombination of



**Fig. 9.** (a) PL spectra and (b) PL delay fitting curves of the BCC50, BiVO<sub>4</sub>, CdS.

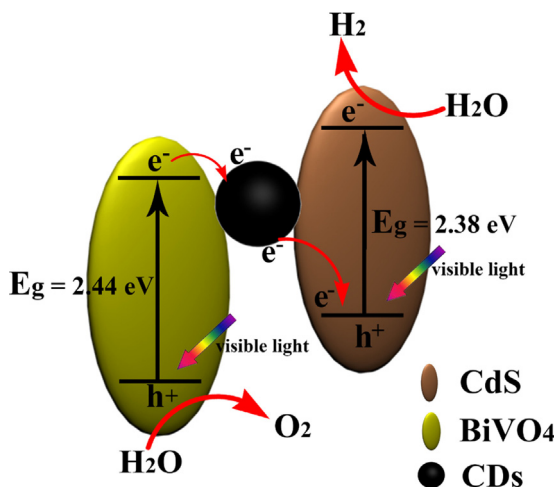


**Fig. 10.** Possible photocatalytic water splitting mechanism of Z-scheme BiVO<sub>4</sub>/CDS/CdS photocatalyst.

charge carriers and increase the lifetime of electrons and holes, thus the Z-scheme BiVO<sub>4</sub>/CDS/CdS photocatalyst shows enhanced photocatalytic activity for water splitting into H<sub>2</sub> and O<sub>2</sub>.

#### 4. Conclusions

We construct a promising solid-state Z-scheme BiVO<sub>4</sub>/CDS/CdS photocatalyst fabricated by a facile precipitation method, which BiVO<sub>4</sub> and CdS nanoparticles can serve as O<sub>2</sub> evolution photocatalyst and H<sub>2</sub> evolution photocatalyst, respectively, and CDs can be used as solid electron mediator for photocatalytic water splitting under visible-light illumination in the absence of sacrificial reagents. The BiVO<sub>4</sub>/CDS/CdS photocatalyst shows enhanced photocatalytic activity with H<sub>2</sub> evolution rate of 1.24 μmol/h and O<sub>2</sub> evolution rate of about 0.61 μmol/h and improved stability for complete water splitting, owing to reduce the recombination of photoexcited charge carriers and extended lifetime of the corresponding carriers. Our work may provide a new insight for the practical application of CdS in large-scale photocatalytic hydrogen production and a promising approach to construct highly efficient Z-scheme catalysts in complete water splitting.

#### Acknowledgements

This work is supported by the Collaborative Innovation Center of Suzhou Nano Science and Technology, the National Natural Science Foundation of China (51422207, 51132006, 51572179, 21471106, 21501126), the Specialized Research Fund for the Doctoral Program of Higher Education (20123201110018), a Suzhou Planning Project

of Science and Technology (ZXG2012028), and a project funded by the Priority Academic Program Development of Jiangsu Higher Education Institutions (PAPD).

#### References

- [1] Nan Zhang, Min Quan Yang, Siqi Liu, Yugang Sun, Yi-Jun Xu, Chem. Rev. 115 (2015) 10307–10377.
- [2] Kazuhiko Maeda, ACS Catal. 3 (2013) 1486–1503.
- [3] A. Fujishima, K. Honda, Nature 238 (1972) 37.
- [4] Ryoya Kobayashi, Satoshi Tanigawa, Toshihiro Takashima, Bunsho Ohtani, Hiroshi Irie, J. Phys. Chem. C 118 (2014) 22450–22456.
- [5] Akihiko Iwase, Yun Hau Ng, Yoshimi Ishiguro, Akihiko Kudo, Rose Amal, J. Am. Chem. Soc. 133 (2011) 11054–11057.
- [6] Yasuyoshi Sasaki, Hideki Kato, Akihiko Kudo, J. Am. Chem. Soc. 135 (2013) 5441–5449.
- [7] Ping Li, Yong Zhou, Haijin Li, Qinfeng Xu, Xiangguang Meng, Xiaoyong Wang, Min Xiao, Zhigang Zou, Chem. Commun. 51 (2015) 800–803.
- [8] Li J. Zhang, Shuo Li, Bing K. Liu, De J. Wang, Teng F. Xie, ACS Catal. 4 (2014) 3724–3729.
- [9] Songmei Sun, Wenzhong Wang, Dezhi Li, Ling Zhang, Dong Jiang, ACS Catal. 4 (2014) 3498–3503.
- [10] Honglin Li, Ke Yu, Xiang Lei, Bangjun Guo, Hao Fu, Ziqiang Zhu, J. Phys. Chem. C 119 (2015) 22681–22689.
- [11] Chade Lv, Gang Chen, Jingxue Sun, Chunshuang Yan, Hongjun Dong, Chunmei Li, RSC Adv. 5 (2015) 3767–3773.
- [12] Jiye Zhang, Yonghao Wang, Jian Jin, Jun Zhang, Zhang Lin, Feng Huang, Jiaguo Yu, ACS Appl. Mater. Interfaces 5 (2013) 10317–10324.
- [13] Tamita Rakshit, Suvar P. Mondal, Indranil Manna, Samit K. Ray, ACS Appl. Mater. Interfaces 4 (2012) 6085–6095.
- [14] Haitao Li, Zhenhui Kang, Yang Liu, Shuit-Tong Lee, J. Mater. Chem. 22 (2012) 24230–24253.
- [15] Hengchao Zhang, Hai Ming, Suoyuan Lian, Hui Huang, Haitao Li, Lili Zhang, Yang Liu, Zhenhui Kang, Shuit-Tong Lee, Dalton Trans. 40 (2011) 10822–10825.
- [16] Zheng Ma, Hai Ming, Hui Huang, Yang Liu, Zhenhui Kang, New J. Chem. 36 (2012) 861–864.
- [17] Benjamin C.M. Martindale, Georgina A.M. Hutton, Christine A. Caputo, Erwin Reisner, J. Am. Chem. Soc. 137 (2015) 6018–6025.
- [18] Haitao Li, Xiaodie He, Zhenhui Kang, Hui Huang, Yang Liu, Jinglin Liu, Suoyuan Lian, Chi Him A. Tsang, Xiaobao Yang, Shuit-Tong Lee, Angew. Chem. Int. Ed. 49 (2010) 4430–4434.
- [19] Juan Liu, Yang Liu, Naiyun Liu, Yuzhi Han, Xing Zhang, Hui Huang, Yeshehahu Lifshitz, Shuit-Tong Lee, Jun Zhong, Zhenhui Kang, Science 347 (2015) 970–974.
- [20] Jungang Hou, Zheng Wang, Chao Yang, Weilin Zhou, Shuqiang Jiao, Hongmin Zhu, J. Phys. Chem. C 117 (2013) 5132–5141.
- [21] Nagarajan Srinivasan, Etsuo Sakai, Masahiro Miyauchi, ACS Catal. 6 (2016) 2197–2200.
- [22] Xing-Liang Yin, Lei-Lei Li, Wen-Jie Jiang, Yun Zhang, Xiang Zhang, Li-Jun Wan, Jin-Song Hu, ACS Appl. Mater. Interfaces 8 (2016) 15258–15266.
- [23] Hai Ming, Zheng Ma, Y. Liu, Keming Pan, Huang Yu, Fang Wang, Zhenhui Kang, Dalton Trans. 41 (2012) 9526–9531.
- [24] Jihua Zhang, Fengzhu Ren, Mingsen Deng, Yuanxu Wang, Phys. Chem. Chem. Phys. 17 (2015) 10218–10226.
- [25] Haimei Fan, Dejun Wang, Zhipeng Liu, Tengfeng Xie, Yanhong Lin, Dalton Trans. 44 (2015) 11725–11731.
- [26] Li Zhang, Dairong Chen, Xiuling Jiao, J. Phys. Chem. B 110 (2006) 2668–2673.
- [27] Danjun Wang, Huidong Shen, Li Guo, Feng Fu, Yucang Liang, New J. Chem. 40 (2016) 8614–8624.
- [28] Jun Di, Jiexiang Xia, Mengxia Ji, Bin Wang, Sheng Yin, Hui Xu, Zhigang Chen, Huaming Li, Langmuir 32 (2016) 2075–2084.
- [29] Di Tang, Hengchao Zhang, Hui Huang, Ruihua Liu, Yuzhi Han, Yang Liu, Cuiyan Tong, Zhenhui Kang, Dalton Trans. 42 (2013) 6285–6289.

- [30] Yongfu Sun, Yi Xie, Changzheng Wu, Ran Long, *Crys. Growth Des.* 10 (2010) 602–607.
- [31] Dandan Wang, Jie Huang, Xia Li, Ping Yang, Yukou Du, Cynthia M. Goh, Cheng Lu, *J. Mater. Chem. A* 3 (2015) 4195–4202.
- [32] Dingning Ke, Tianyou Peng, Liang Ma, Ping Cai, Ke Dai, *Inorg. Chem.* 48 (2009) 4685–4691.
- [33] R. Kanagadurai, R. Sankar, G. Sivanesan, S. Srinivasan, R. Rajasekaran, R. Jayavel, *Mater. Chem. Phys.* 108 (2008) 170–175.
- [34] Jingbin Liu, Hao Wang, Shu Wang, Hui Yan, *Mater. Sci. Eng. B* 104 (2003) 36–39.
- [35] Yong Liu, Kai Yan, Jingdong Zhang, *ACS Appl. Mater. Interfaces* 8 (2016) 28255–28264.
- [36] Fang Jiang, Tingting Yan, Huan Chen, Aiwu Sun, Chenmin Xu, Xin Wang, *Appl. Surf. Sci.* 295 (2014) 164–172.
- [37] Xiuqin Wu, Juan Zhao, Sijie Guo, Liping Wang, Weilong Shi, Hui Huang, Yang Liu, Zhenhui Kang, *Nanoscale* 8 (2016) 17314–17321.
- [38] MingWei Xiao, LiShi Wang, YanDan Wu, Xinjian Huang, Zhi Dang, *Nanotechnology* 19 (1) (2007) 015706.
- [39] Rajesh Bera, Simanta Kundu, Amitava Patra, *ACS Appl. Mater. Interfaces* 7 (2015) 13251–13259.
- [40] Lei Zhou, Juan Liu, Xing Zhang, Ruihua Liu, Hui Huang, Yang Liu, Zhenhui Kang, *Nanoscale* 6 (2014) 5831–5837.
- [41] Juanjuan Sun, Xinyong Li, Qidong Zhao, Moses O. Tadé, Shaomin Liu, *J. Mater. Chem. A* 3 (2015) 21655–21663.
- [42] Daluo Peng, Huihu Wang, Kun Yu, Ying Chang, Xinguo Ma, Shijie Dong, *RSC Adv.* 6 (2016) 77760–77767.
- [43] Xue Lin, Yushuang Wang, Jia Zheng, Chang Liu, Yang Yang, Guangbo Che, *Dalton Trans.* 44 (2015) 19185–19193.
- [44] Libang Kuai, Yong Zhou, Wengguang Tu, Ping Li, Haijin Li, Qin Feng Xu, Lanqin Tang, Xiaoyong Wang, Min Xiao, Zhigang Zou, *RSC Adv.* 5 (2015) 88409–88413.
- [45] Yinzhou Wang, Wei Wang, Hongying Mao, Yunhao Lu, Jianguo Lu, Jingyun Huang, Zhizhen Ye, Bin Lu, *ACS Appl. Mater. Interfaces* 6 (2014) 12698–12706.
- [46] Sang Hee Yun, Pravin G. Ingole, Won Kil Choi, Jong Hak Kim, Hyung Keun Lee, *J. Mater. Chem. 3* (2015) 7888–7899.
- [47] Zichao Lian, Pengpeng Xu, Wencho Wang, Dieqing Zhang, Shuning Xiao, Xin Li, Guisheng Li, *ACS Appl. Mater. Interfaces* 7 (2015) 4533–4540.
- [48] Pan-Yong Kuang, Yu-Zhi Su, Kang Xiao, Zhao-Qing Liu, Nan Li, Hong-Juan Wang, Jun Zhang, *ACS Appl. Mater. Interfaces* 7 (2015) 16387–16394.
- [49] Subramanian Balachandran, Natarajan Prakash, Kuppulingam Thirumalai, Manickavachagan Muruganandham, Mika Sillanpää, Meenakshisundaram Swaminathan, *Ind. Eng. Chem. Res.* 53 (2014) 8346–8356.
- [50] Ya Liu, Ping Zhang, Baozhu Tian, Jinlong Zhang, *ACS Appl. Mater. Interfaces* 7 (2015) 13849–13858.
- [51] Juanjuan Sun, Xinyong Li, Qidong Zhao, Jun Ke, Dongke Zhang, *J. Phys. Chem. C* 118 (2014) 10113–10121.
- [52] Yangyang Zhang, Yiping Guo, Huanan Duan, Hua Li, Chongyang Sun, Hezhou Liu, *Phys. Chem. Chem. Phys.* 16 (2014) 24519–24526.
- [53] Fan Qi Zhou, Jin Chen Fan, Qun Jie Xu, Yu Lin Min, *Appl. Catal. B: Environ.* 201 (2017) 77–83.
- [54] Nan Zhang, Yanhui Zhang, Xiaoyang Pan, Xianzhi Fu, Siqi Liu, Yi-Jun Xu, *J. Phys. Chem. C* 115 (2011) 23501–23511.
- [55] Jonghun Lim, Damián Monllor-Satoca, Jum Suk Jang, Seockheon Lee, Wonyong Choi, *Appl. Catal. B: Environ.* 152 (2014) 233–240.
- [56] Yiming He, Lihong Zhang, Botao Teng, Maohong Fan, *Environ. Sci. Technol.* 49 (2015) 649–656.
- [57] Ruibin Liu, Lijie Shi, Bingsuo Zou, *ACS Appl. Mater. Interfaces* 6 (2014) 10353–10366.
- [58] Xin Wang, Li Cao, Fushen Lu, Mohammed J. Meziani, Heting Li, Gang Qi, Bing Zhou, Barbara A. Harruff, Fabien Kermarrec, Ya-Ping Sun, *Chem. Commun.* (2009) 3774–3776.
- [59] Haitao Li, Ruihua Liu, Suoyuan Lian, Yang Liu, Hui Huang, Zhenhui Kang, *Nanoscale* 5 (2013) 3289–3297.